CHEMISTRY
A EUROPEAN JOURNAL

ChemPubSoc Europe

DOI: 10.1002/chem.201300010

Axis-Oriented, Continuous Anatase Titania Films with Exposed Reactive {100} Facets

Thanh-Khue Van, Cuong Ky Nguyen, and Young Soo Kang*[a]

Abstract: Homogeneous TiO_2 single crystals with high exposure of {100} reactive facets were constructed as a seed monolayer on transparent conductive substrates with the desired orientation of reactive facets. A secondary growth process was subsequently carried out on the monolayer seed film to form an axis-oriented continuous reactive film. Performing secondary growth with different precursors led to optimized conditions for high-performance photoelectrochemical activity of anatase TiO_2 films. Experimental techniques such as UV/Vis absorption spectroscopy, X-ray diffraction, high-resolution SEM, and photoelectrochemistry were used to characterize the structural, optical, and photoelectrochemical properties of the as-synthesized films. As a photoanode in a photoelectrochemical cell, the axis-oriented reactive film shows a maximum photocurrent density of $0.3\,mA\,cm^{-2}$, as opposed to $0.075\,mA\,cm^{-2}$ for non-axis-oriented (randomly oriented) TiO_2 film.

Keywords: crystal growth · electrochemistry · nanoparticles · photochemistry · thin films

Introduction

Nanotechnology with shape or morphology control for photocatalysts is at the dawn of its age, and great achievements in understanding, applying, and especially fabricating nanomaterials have been made in the last decades. From spherical or simple morphologies in the early days, the synthesis of nanomaterial with complicated or polyhedral shapes (rod, tripodlike, flakelike, truncated hexagonal bipyramid, etc.) has become increasingly common nowadays. Assembly of metal or semiconductor nanoparticles in monolayer films has created intriguing opportunities for exploring multifunctional properties and applications. However, the well-known vacuum techniques for in situ preparation of highly oriented semiconductor thin films, such as molecular beam epitaxy, pulsed-laser deposition, metal–organic chemical vapor deposition, vapor–liquid–solid method, and surface templation, have been used in only few limited or specific cases.[1–4] Recently, manual assembly[5] and secondary growth[6] of seed layers under hydrothermal conditions have enabled the exploration of new methods in the fabrication of semiconductor nanocrystal thin-film arrays by oriented assembly of nano- and microcrystals.

Undoubtedly, TiO_2 was the first and is still the most widely used photocatalytic material because of its biological and chemical inertness, strong oxidizing power, cost effectiveness, long-term stability against photo- and chemical corrosion, and availability of source materials.[7,8] Since the first report on anatase TiO_2 single crystals with 47% exposed {001} facets,[9] many studies have been conducted to synthesize differently shaped and free-standing anatase TiO_2 single crystals with exposed {001}[10–16] and {100} facets.[10,17–21] However, these reactive facets are only relevant to applications such as photovoltaics and photodissociation of water once they are in form of TiO_2 thin films, preferably deposited on transparent conductive substrates. Although many chemical and physical methods have been investigated for preparing anatase TiO_2 films,[2,7,8,22–26] including axis-oriented films with highly reactive {001} anatase facets,[27,28] deposition of oriented films with {100} facets has not been realized yet. Herein, we report the facile fabrication and characterization of {100}-oriented thin films of anatase TiO_2 nanocrystal array on a transparent conductive substrate by a combination of manual assembly and secondary growth (Scheme 1).

Results and Discussion

The synthesis of {100} anatase TiO_2 single crystals was based on our recently reported method.[21] The effects of surfactant additives such as cetyltrimethylammonium bromide (CTAB) and sodium dodecyl benzenesulfonate (SDBS) on the morphology control of TiO_2 single crystals were studied in this work. Figure 1 shows an overview of the as-synthesized products. In the presence of CTAB, uniform cubic-shaped crystals (Figure 1a and b), which are illustrated schematically in the inset, were obtained in high yield. This particle shape exposes large rectangular lateral {100} facets and

[a] T.-K. Van,[+] C. K. Nguyen,[+] Prof. Y. S. Kang
Korea Center for Artificial Photosynthesis
Department of Chemistry, Sogang University
Seoul (Korea)
Fax: (+82) 2-701-0967
E-mail: yskang@sogang.ac.kr

[+] These authors contributed equally to this work.

Supporting information for this article is available on the WWW under http://dx.doi.org/10.1002/chem.201300010.

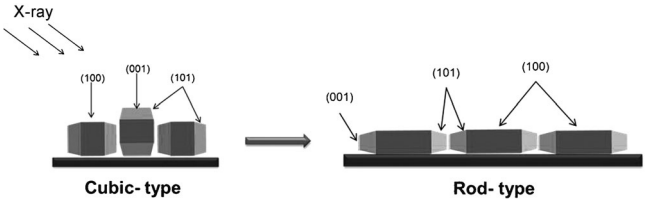

Scheme 1. Schematic illustration of the orientation ({100} exposure) of monolayers assembled from differently shaped particles.

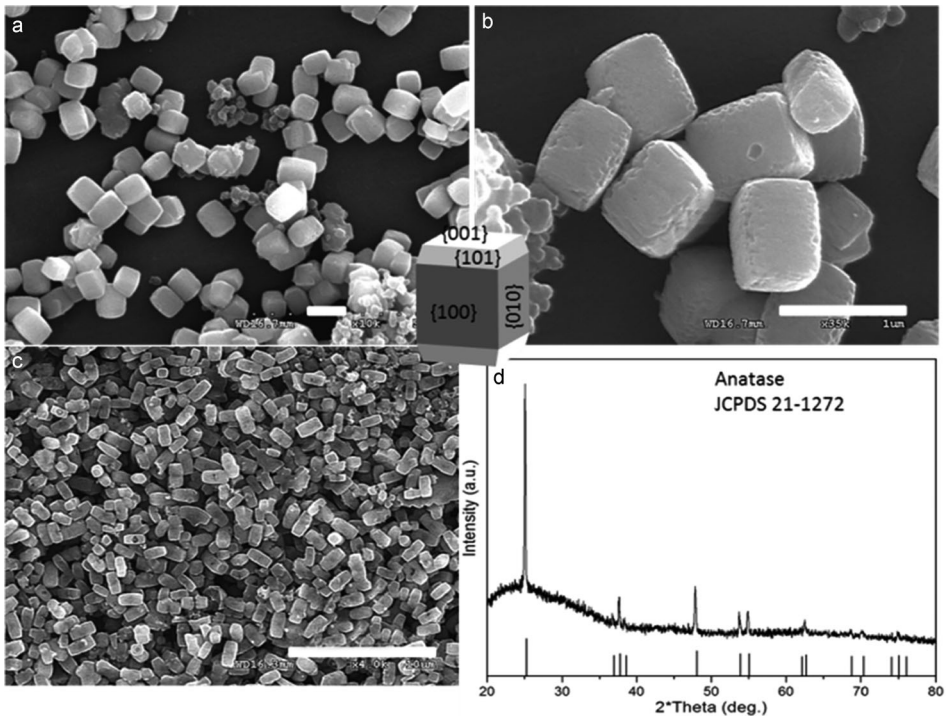

Figure 1. a), b) SEM images of the cubic-type {100} TiO_2 crystals prepared by a CTAB-assisted process. c) Rod-type {100} particles prepared by an SDBS-assisted process. d) XRD patterns of TiO_2 products. Scale bars: a), b) 1 μm, and c) 10 μm.

square top {001} facets. On the other hand, uniform rodlike particles (Figure 1c) were obtained with SDBS. Compared with the cubic crystals, these particles are elongated along the {001} axis to form a rod-type morphology with expansion of the four {100} lateral facets. The diffraction peaks of the as-synthesized particles match well with the crystal structure of the anatase TiO_2 phase (JCPDS No. 21-1272), and no residual Ti phase could be detected (Figure 1d). The formation of uniform cubelike TiO_2 particles is highly dependent on the presence of CTAB acting as a surfactant in the system. An electrostatic interaction took place between CTA^+ cations and $[Ti(OH)_6]^{2-}$ anions in the initial steps of hydrolysis, and the negative sites in the TiO_2 surfaces were fully close packed with CTA^+. Moreover, the interaction between CTAB and the anionic surfactant CMC enhances the adsorption of both CTAB and CMC on titania particles. These effects decrease the rates of hydrolysis and diffusion, and thus lead to more adsorption of fluoride ions on the surfaces of the TiO_2 crystals, which decreases the surface energy more effectively on {001} and {100} facets. Thus, the percentage of {101} facets is reduced in comparison with other anatase single crystals. Moreover, adsorption of surfactants also suppresses agglomeration of crystals. The anionic surfactant SDBS is selectively adsorbed on the positively polarized surface of anatase TiO_2 crystals by electrostatic interactions. Competitive adsorption between DBS^- anions and fluorine ions on the five-coordinate titanium Ti_{5c} atoms of TiO_2 surfaces (positively polarized sites) would occur. The {001} facets, which have the highest density of Ti_{5c},[29] would mainly adsorb SDBS, so the excess fluorine anions would have to be adsorbed on other facets. Thus, the surface energy of {100} facets was decreased greatly, and rod-type single crystals with large exposed {100} facets were formed.

Applications of the reactive facets in photovoltaics or photocatalysts for water splitting with potentially high performance are expected if only these facets are exposed under photoillumination. By using the manual assembly method,[5] the as-synthesized TiO_2 single crystals were assembled with good close packing on fluorine-doped tin oxide (FTO) glass as a seed monolayer. Figure 2a and b show monolayer thin films of the as-synthesized TiO_2 particles with dominant axis-oriented reactive facets on FTO glass substrates. The rod-type TiO_2 particles with higher percentage of {100} facets give much better close-packed and well-oriented monolayer film arrays than the cubic-type TiO_2 crystals due to their geometric shape (see Scheme 1). The better axis orientation of the rod-type monolayer is confirmed by the XRD patterns in Figure 2c, which show enhanced intensity of the (200) diffraction peak compared with its standard intensity and that of the cubic-type crystals, which can be rationalized by considering that most of rod-type particles are enclosed by larger lateral {100} facets and smaller top {001} facets, so their lateral {100} facets lie on the substrate surface. The monolayer array of rod-type single crystals also exhibits better photoactivity than its cubic-type counterpart (Figure 2d). This could be on account of the higher percentage of exposed {100} facets and better close packing.

We expected that the photoactivity of the film could be enhanced by filling the gaps between particles to give a continuous film while maintaining the {100} oriented facets. Hence, we carried out a secondary growth (SG) reaction on

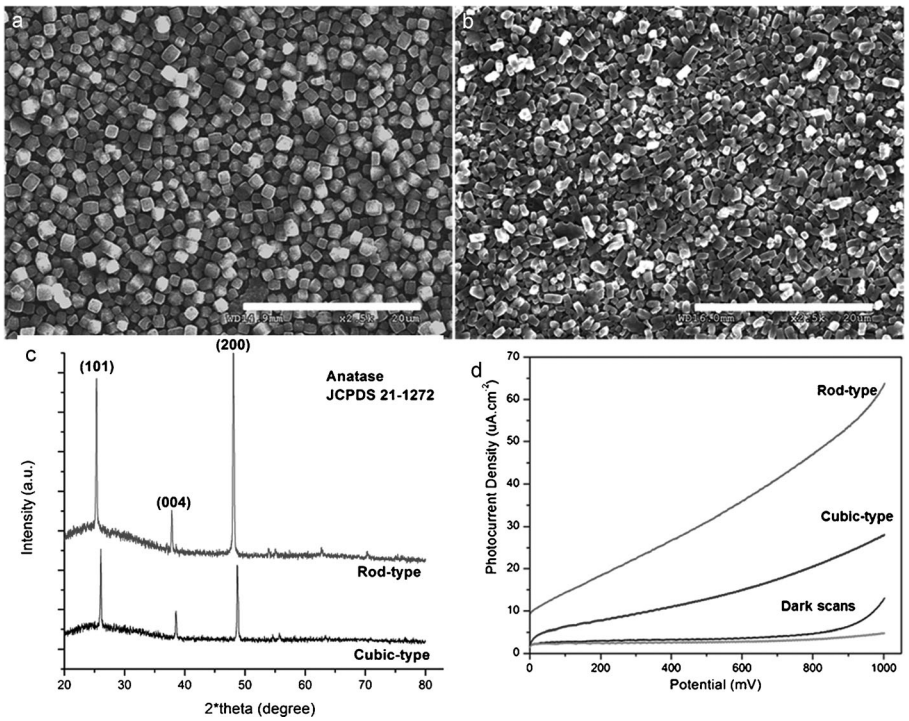

Figure 2. SEM images of the axis-oriented monolayer films of a) cubic-type and b) rod-type TiO_2 single crystals. c) XRD patterns of the monolayers on glass substrates. d) Photoelectrochemical properties of the TiO_2 particle monolayer films.

the monolayer film of rod-type TiO_2 seeds. The different components of reactant were also examined. An as-produced film with clear grain boundaries could be observed when $TiCl_3$ was used as sole reactant in the SG reaction solution (see Figure S1a in the Supporting Information). The roughness of the particle film is an effect of the SG process. As shown in Figure S1b in the Supporting Information, the presence of HF in the reaction mixture, which increases the pH of the solution, prevents the seed crystals from dissolving in the strongly acidic environment due to the content of HCl in the original precursor solution. Addition of CMC did not give a better film morphology (see Figure S1c in the Supporting Information), but led to interesting optical and photocatalytic properties. The visual appearance and optical behavior of the films obtained with and without CMC are shown in Figure S2a in the Supporting Information, which reveals that the bare TiO_2 film (sample 1) absorbs only UV light, whereas the brown TiO_2 films (samples 2 and 3) show large optical absorbance in the visible-light region. The two brown samples probably underwent a C-doping process, which changed the color and absorption band of TiO_2. Wu et al. reported a similar C-doping process through degradation of glucose during hydrothermal treatment.[30] The narrower bandgap of C-doped TiO_2 enhances solar-energy harvesting and thus results in better visible-light photocatalytic activity compared to pristine TiO_2 (see Figure S2b in the Supporting Information). Sample 3, which had a higher concentration of Ti precursor, shows a darker color, better visible-light absorption, and superior photoelectrochemical properties. This can be explained by incorporation of a larger amount of carbon into the newly formed TiO_2 film by interaction with the Ti and O atoms of TiO_2. Although this is an interesting method to create C-doped TiO_2 films, the true photoactivity of {100}-oriented film is still not well defined due to random orientation of the obtained film. It was therefore necessary to find another method to fabricate {100} axis-oriented TiO_2 films, and use of $Ti(OBu)_4$ as precursor was the solution. Combining the mild chemical reactivity of $Ti(OBu)_4$ under solvothermal conditions and a relatively slow reaction rate would be a suitable way to fabricate TiO_2 films while maintaining the axis orientation. Figure S3 (see Supporting Information) shows an axis-oriented continuous TiO_2 film obtained by an SG process with $Ti(OBu)_4$ precursor. The exposed {100} facets are rough and look like a growing construction of nanosheets. The effect of the initial reactant concentration on the quality of SG film was also studied. Figure 3 shows that the roughness and close packing of the surface of the growing film could be varied dramatically by increasing the initial $Ti(OBu)_4$ content in the SG solution from 2.67 to 13.33 mM. Apparently, when the concentration of titanium precursor is low, the SG of layered seeds is not as homogenous as at higher concentration due to equilibrium between crystallization and dissolution.

A comparison of morphology and photocurrent density of TiO_2 films is presented in Figure S4 of the Supporting Information. The monolayer film of TiO_2 particles with {100}-axis orientation (see Figure S4a in the Supporting Information) exhibits the lowest photocurrent density, which could be due to the weak contact between the layer of particles and the FTO substrate. That is attributed to partial trapping of the photogenerated charge carriers transferred to the outer circuit. Although the continuous, randomly oriented film (see Figure S4b in the Supporting Information) has good interaction with FTO, the disappearance of reactive facets after the SG process results in only minor improvements in photoactivity. Interestingly, we observed a greatly enhanced photocurrent density (see Figure S4d in the Supporting Information) for the SG TiO_2 film with continuity and {100}-axis orientation. This significant enhancement is attributed to both good adhesion between the TiO_2 film and FTO, as is demonstrated in Figure S3b in the Supporting Information, and

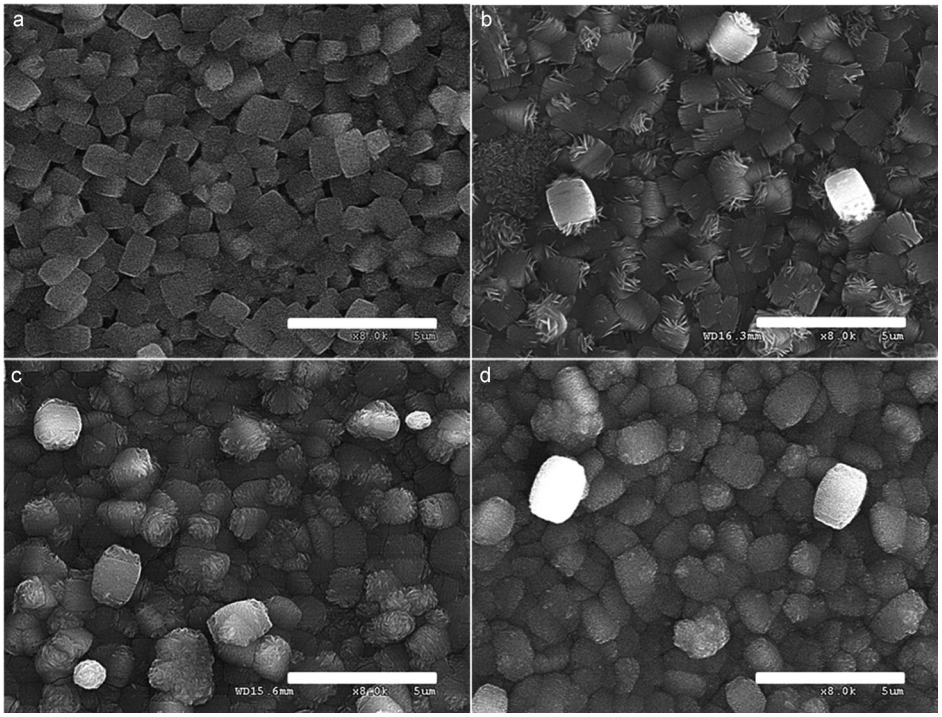

Figure 3. SEM images of SG films obtained with different concentrations of $Ti(OBu)_4$. a) 2.67, b) 5.33, c) 10.67, and d) 13.33 mM. Scale bars: 5 μm.

the exposure of photoreactive {100} facets on the film (see Figure S4c in the Supporting Information).

The photoelectrochemical properties of SG TiO_2 films are also strongly dependent on post-growth heat treatment (see Figure S5 in the Supporting Information). Under illumination, electrons and holes are generated within the semiconductor film, and the photoinduced electrons are transferred to the FTO substrate and move in the outer circuit and then to the cathode. In low-crystallinity films, this would cause a decrease in photoelectron transfer rate of these charge carriers within the film and gradually decrease the photocurrent during illumination (see Figure S5a in the Supporting Information). Post-growth annealing not only improves the crystallinity of the film, and hence the stability during illumination, but also enhances the photoefficiency of SG films, for example, from 170 to 300 $\mu A\,cm^{-2}$ for sample 3. The photoresponse spike of the annealed samples apparently show the immediate response to initial illumination as photogenerated electron–hole pairs and then decreases to a steady-state value. The observed decay profile can be attributed to recombination of charge carriers at defect sites in the TiO_2 films.

Conclusion

A combination of manual assembly and secondary growth was applied to prepare continuous ordered anatase TiO_2 crystal monolayer films with {100}-axis orientation on FTO substrates. First, anatase TiO_2 single crystals with exposed {100} facets were axis-oriented on suitable substrates; second, a secondary growth process was used to fill the gaps between particles and connect the particle layer to the substrate while retaining the desired facet orientation. This combination methodology also provides a promising method for in situ doping of TiO_2 films with elements. The obtained {100}-facet-oriented continuous anatase film demonstrated high photoactivity even in visible light (photocurrent density $0.3\,mA\,cm^{-2}$ at 1.0 V vs. Ag/AgCl). This higher photoactivity compared to the randomly oriented sample can be achieved for anatase TiO_2 only by oriented exposure of the {100} facets over the whole film surface.

Experimental Section

Synthesis of anatase single crystals with {100} facets: In a typical synthetic procedure, an aqueous solution of titanium trichloride (30 mL, 5.33 M, Aldrich), carboxymethyl cellulose, sodium salt (CMC, $2.8\,g\,L^{-1}$, $M_w = 90000$), and hydrofluoric acid (0.4 mL, 10 wt%) were added to a Teflon-lined autoclave, and a green transparent mixture was formed. The surfactant additive cetyltrimethylammonium bromide (CTAB, $1.4\,g\,L^{-1}$) or sodium dodecyl benzenesulfonate (SDBS, $1.4\,g\,L^{-1}$) was initially mixed with the reaction solution to form a transparent homogenous solution. The sealed autoclave was then put in an oven for hydrothermal treatment at 180 °C for 10 h. Subsequently, the reaction mixture was cooled under a water shower. The uniform and single-crystalline as-synthesized product was collected by centrifugation and washed with copious distilled deionized water (DDW) and ethyl alcohol several times to remove dissolvable ionic impurities. The samples were then dried at 80 °C in air.

Fluorine removal from the surface of anatase TiO_2 single crystals: Typically, the as-prepared {100} anatase TiO_2 single-crystal nanoparticles were heated in static air in a muffle furnace at 500 °C for 3 h with a ramping rate of $5\,°C\,min^{-1}$ and then allowed to cool to room temperature for further characterization. Both fluorine and organic contaminants were removed in this process.

Preparation of {100} facet-oriented anatase TiO_2 film: F-doped tin oxide (FTO) glass substrate (20×20 mm) was rinsed with 3 wt% Mucasol solution and then with copious DDW. The clean substrates were spin-coated with 2.0 wt% polyethyleneimine (PEI, $M_w = 25000$) at a speed of 2000 rpm for 15 s. The as-synthesized {100} anatase particles were placed on the PEI-coated substrates and rubbed by a finger smoothly for a while. The amounts of rod-type and cubic-type TiO_2 crystals loaded on substrates were calculated as shown in Table 1 (see Supporting Information). The single-axis oriented monolayer film was calcined at 500 °C for 3 h to remove the polymeric linker and to improve the adhesion between titania crystals and substrate. The subsequent secondary growth process was carried out on these films as follows. The calcined monolayer film

was immersed into a 30 mL of a solution of secondary growth reaction gel, sealed in a Teflon-lined autoclave and then heated at 180 °C for 10 h under static conditions in an oven. The resulting axis-oriented anatase TiO_2 thin film was repeatedly calcined at 400 °C for 2 h to increase film's crystalline behavior.

Measurement and characterization: Crystallographic data of anatase TiO_2 single crystals were obtained by XRD (Rigaku miniFlex-II desktop X-ray diffractometer, $Cu_{K\alpha}$ radiation with $\lambda = 0.154056$ nm). Morphologies of anatase TiO_2 single-crystal powders and films were observed by SEM (Hitachi S-4300 FE-SEM). UV/Vis absorption spectra of the samples were recorded on a Varian Cary 5000 UV/Vis/NIR spectrophotometer equipped with an integrating sphere. Photoelectrochemical measurements on TiO_2 thin-film electrodes (diameter: 0.7 cm, area: 0.38 cm^2) as photoanode were conducted with a PL-9 potentiostat in a conventional three-electrode system in a V-style with quartz-window cell at room temperature under 1 Sun (Asahi HAL-320, 100 $mW\,cm^{-2}$) illumination, with a Pt foil and an Ag/AgCl electrode as counter- and reference electrodes, respectively. Photocurrent–potential (*I–V*) curves were obtained by linear sweep voltammetry with a scan rate of 20 $mV\,s^{-2}$. Na_2SO_4 (0.5 M, pH 6.3) was used as electrolyte solution. Photoresponses were measured by chronoamperometry at a constant potential of 1.0 V. The potentials are reported versus Ag/AgCl (measured) or RHE (obtained by using the relationship $E_{Ag/AgCl} = E_{RHE} - 0.0591\,pH - 0.1976$ V).

Acknowledgements

This work was supported by the Korea Center for Artificial Photosynthesis (KCAP) located in Sogang University funded by the Ministry of Education, Science, and Technology (MEST) through the National Research Foundation of Korea (No. 2012M1A2A2671783).

[1] a) L. E. Greene, M. Law, D. H. Tan, M. Montano, J. Goldberger, G. Somorjai, P. Yang, *Nano Lett.* **2005**, *5*, 1231; b) L. E. Greene, M. Law, J. Goldberger, F. Kim, J. C. Johnson, Y. Zhang, R. J. Saykally, P. Yang, *Angew. Chem.* **2003**, *115*, 3139; *Angew. Chem. Int. Ed.* **2003**, *42*, 3031.
[2] X. Feng, K. Shankar, O. K. Varghese, M. Paulose, T. J. Latempa, C. A. Grimes, *Nano Lett.* **2008**, *8*, 3781.
[3] a) A. M. Morales, C. M. Lieber, *Science* **1998**, *279*, 208; b) J. D. Holmes, K. P. Johnston, R. C. Doty, B. A. Korgel, *Science* **2000**, *287*, 1471.
[4] a) H. Q. Cao, Y. Xu, J. M. Hong, H. B. Liu, G. Yin, B. L. Li, C. Y. Tie, Z. Xu, *Adv. Mater.* **2001**, *13*, 1393; b) X. Duan, C. Niu, V. Sahi, J. Chen, J. W. Parce, S. Empedocles, J. L. Goldman, *Nature* **2003**, *425*, 274.
[5] J. S. Lee, J. H. Kim, Y. J. Lee, N. C. Jeong, K. B. Yoon, *Angew. Chem.* **2007**, *119*, 3147; *Angew. Chem. Int. Ed.* **2007**, *46*, 3087.
[6] Z. Lai, G. Bonilla, I. Diaz, J. G. Nery, K. Sujaoti, M. A. Amat, E. Kokkoli, O. Terasaki, R. W. Thompson, M. Tsapatsis, D. G. Vlachos, *Science* **2003**, *300*, 456.
[7] X. Chen, S. S. Mao, *Chem. Rev.* **2007**, *107*, 2891.
[8] X. Chen, *Chin. J. Catal.* **2009**, *30*, 83.
[9] H. G. Yang, C. H. Sun, S. Z. Qiao, J. Zou, G. Liu, S. C. Smith, H. M. Cheng, G. Q. Lu, *Nature* **2008**, *453*, 638.
[10] B. H. Wu, C. Y. Guo, N. F. Zheng, Z. X. Xie, G. D. Stucky, *J. Am. Chem. Soc.* **2008**, *130*, 17563.
[11] H. G. Yang, G. Liu, S. Z. Qiao, C. H. Sun, Y. G. Jin, S. C. Smith, J. Zou, H. M. Cheng, G. Q. Lu, *J. Am. Chem. Soc.* **2009**, *131*, 4078.
[12] X. G. Han, Q. Kuang, M. S. Jin, Z. X. Xie, L. S. Zheng, *J. Am. Chem. Soc.* **2009**, *131*, 3152.
[13] Y. Q. Dai, C. M. Cobley, J. Zeng, Y. M. Sun, Y. N. Xia, *Nano Lett.* **2009**, *9*, 2455.
[14] G. Liu, H. G. Yang, X. W. Wang, L. N. Cheng, J. Pan, G. Q. Lu, H. M. Cheng, *J. Am. Chem. Soc.* **2009**, *131*, 12868.
[15] D. Q. Zhang, G. S. Li, X. F. Yang, J. C. Yu, *Chem. Commun.* **2009**, 4381.
[16] J. S. Cheng, Y. L. Tan, C. M. Li, Y. L. Cheah, D. Y. Luan, S. Madhavi, F. Y. C. Boey, L. A. Archer, X. W. Lou, *J. Am. Chem. Soc.* **2010**, *132*, 6124.
[17] P. Wen, H. Itoh, W. Tang, Q. Feng, *Langmuir* **2007**, *23*, 11782.
[18] C.-T. Dinh, T.-D. Nguyen, F. Kleitz, T.-O. Do, *ACS Nano* **2009**, *3*, 3737.
[19] J. Li, D. Xu, *Chem. Commun.* **2010**, *46*, 2301.
[20] J. Pan, G. Liu, G. Q. Lu, H.-M. Cheng, *Angew. Chem.* **2011**, *123*, 2181; *Angew. Chem. Int. Ed.* **2011**, *50*, 2133.
[21] C. K. Nguyen, H. G. Cha, Y. S. Kang, *Cryst. Growth Des.* **2011**, *11*, 3947.
[22] a) H. Pizem, C. N. Sukenik, *Chem. Mater.* **2002**, *14*, 2476; b) Y. Masuda, T. Sugiyama, W. S. Seo, K. Koumoto, *Chem. Mater.* **2003**, *15*, 2469; c) S. Yamabi, H. Imai, *Chem. Mater.* **2002**, *14*, 609.
[23] a) J.-J. Wu, C.-C. Yu, *J. Phys. Chem. B* **2004**, *108*, 3377; b) E. Hosono, S. Fujihara, K. Kakiuchi, H. Imai, *J. Am. Chem. Soc.* **2004**, *126*, 7790; c) X. J. Feng, J. Zhai, L. Jiang, *Angew. Chem.* **2005**, *117*, 5245; *Angew. Chem. Int. Ed.* **2005**, *44*, 5115.
[24] a) D. H. Wang, J. Liu, Q. S. Huo, Z. M. Nie, W. G. Lu, R. E. Williford, Y.-B. Jiang, *J. Am. Chem. Soc.* **2006**, *128*, 13670; b) S. P. Albu, A. Ghicov, J. M. Macak, R. Hahn, P. Schmuki, *Nano Lett.* **2007**, *7*, 1286.
[25] a) Y. Li, T. Sasaki, Y. Shimizu, N. Koshizaki, *J. Am. Chem. Soc.* **2008**, *130*, 14755; b) B. Liu, J. E. Boercker, E. S. Aydil, *Nanotechnology* **2008**, *19*, 505604.
[26] a) O. K. Varghese, M. Paulose, C. A. Grimes, *Nat. Nanotechnol.* **2009**, *4*, 592; b) A. I. Hochbaum, P. D. Yang, *Chem. Rev.* **2010**, *110*, 527; c) B. Liu, E. S. Aydil, *J. Am. Chem. Soc.* **2009**, *131*, 3985.
[27] X. Wang, G. Liu, L. Wang, J. Pan, G. Q. Lu, H. M. Cheng, *J. Mater. Chem.* **2011**, *21*, 869.
[28] B. Liu, E. S. Aydil, *Chem. Commun.* **2011**, *47*, 9507.
[29] a) M. Lazzeri, A. Vittadini, A. Selloni, *Phys. Rev. B* **2001**, *63*, 155409; b) M. Lazzeri, A. Vittadini, A. Selloni, *Phys. Rev. B* **2002**, *65*, 119901.
[30] F. Dong, H. Wang, Z. Wu, *J. Phys. Chem. C* **2009**, *113*, 16717.

Received: January 2, 2013
Revised: April 9, 2013
Published online: June 3, 2013

